Plasma-nitriding and characterization of FeAl40 iron aluminide

Zhang, Zhenxue; Li, Xiaoying; Dong, Hanshan

DOI:
10.1016/j.actamat.2014.11.044

Document Version
Publisher's PDF, also known as Version of record

Citation for published version (Harvard):
Zhang, Z, Li, X & Dong, H 2015, 'Plasma-nitriding and characterization of FeAl40 iron aluminide', *Acta Materialia*, vol. 86, pp. 341-351. https://doi.org/10.1016/j.actamat.2014.11.044

Available online at www.sciencedirect.com

ScienceDirect

Acta Materialia 86 (2015) 341–351

Acta MATERIALIA

www.elsevier.com/locate/actamat

Plasma-nitriding and characterization of FeAl40 iron aluminide

Zhenxue Zhang, Xiaoying Li* and Hanshan Dong

School of Metallurgy and Materials, The University of Birmingham, Birmingham B15 2TT, UK

Received 9 September 2014; revised 17 November 2014; accepted 24 November 2014

Abstract—The response to plasma-nitriding of a B2 FeAl40 aluminide was investigated in this work using varying temperatures, times and gas mixtures. The microstructure of the plasma-nitrided cases were fully characterized using glow discharge optical emission spectroscopy, scanning electron microscopy/energy-dispersive X-ray spectroscopy, X-ray diffraction and transmission electron microscopy, as well as microhardness testing. Based on the experimental results, the observed abnormal growth kinetics of the nitride case formed at 700 °C was investigated and a model was put forward to understand the mechanism involved in the formation of wave-like line features within the nitride cases.

Keywords: Plasma-nitriding; Iron aluminide; Aluminium nitride

1. Introduction

The ever-increasing demands for high performance, high energy efficiency and low environmental impact have been the main driver for the development of intermetallic materials in view of their unique properties at elevated temperatures. Iron aluminides, initially developed for high temperature applications in the aerospace industry, have in recent years attracted considerable scientific and technological interest in medium-to-high temperature non-aerospace applications (e.g. for the automotive industry) owing to their unique combination of outstanding high-temperature oxidation and good corrosion resistance in various aggressive environments, relatively low materials density (5.76–6.32 g cm^{-3}) compared with commercial stainless steels and nickel-based alloys and good mechanical properties (strength, stiffness and creep resistance) at temperatures up to 800 °C [1]. These advantages have led to several potential applications, including automobile and other industrial valve components, catalytic converter substrates and components for molten salt applications [2]. Due to their special characteristics, iron aluminides have also been used as surface materials via different surface engineering technologies, such as thermal spraying [3], laser surface cladding technology [4] and chemical vapour deposition [5] etc.

Great progress has been made in the past in improving the mechanical properties of the bulk iron aluminides in terms of room temperature toughness, ductility and fracture behaviour, high-temperature strength and creep resistance via microalloying, grain size reduction and advanced materials processing as well as heat treatment [6–10]. For example, based on oxide (Y_2O_3) dispersion strengthening (ODS), powder metallurgy (P/M) and hot extrusion, a new generation of B2 FeAl alloy has been developed with significantly enhanced room temperature ductility (12–15% in air) [11]. This has paved the way for such structural applications of iron aluminides as automotive and die-and-tool components [12]. Unfortunately, research has also shown that wear resistance of the iron aluminides is not as high as most of stainless steels [13–15], which could impede their future tribological applications when wear and surface contact are involved such as valves in a car engine. To this end, a few studies were carried out to investigate the influence of the addition of carbon, or secondary hard particles such as WC, TiB_2 and TiC, on the wear performance of bulk iron aluminide materials [16,17] whilst some studies were directed at improving the tribological properties of Fe–Al intermetallics via a surface engineering approach.

The advanced ceramic conversion technique developed by Li and Dong [18] has been successfully applied to improve the surface hardness and wear resistance of Fe–Al intermetallics by converting the surface into a hard (~23 GPa) and adherent Al_2O_3 layer [19]. Significant improvement in wear resistance has been achieved under a low-to-medium load but severe layer cracking under a high load was observed, i.e. the "thin-ice effect", because of the very thin (<3 μm) ceramic layer without appropriate diffusion zone underneath. Boronizing [20] and low energy–high flux nitridation treatment [21,22] were also investigated to

* Corresponding author. Tel.: +44 1214147105; e-mail addresses: x.li.1@bham.ac.uk; donglixy@gmail.com

http://dx.doi.org/10.1016/j.actamat.2014.11.044
1359-6462/

enhance the wear resistance but the modified layer is still too thin for high load applications.

Recently, Spies et al. [23] conducted a series of gas nitriding treatments of FeAl intermetallic alloys at temperatures between 450 and 850 °C. It was found that the thickness of the nitrided layers increased with increasing the treatment temperature up to 650 °C, and a further increase in temperature resulted in considerable decrease of the layer thickness. The authors claimed that this abnormal growth kinetics could be related to the reduced thermal decomposition of NH_3 at temperatures above 650 °C. However, our work indicated that such abnormal growth kinetics also occurred during plasma-nitriding of FeAl alloy although a mixture of N_2 and H_2 (rather than NH_3) was used in our plasma-nitriding. Clearly, the assumption by Spies et al. cannot be used to explain the abnormal growth kinetics observed in plasma-nitriding, and there must be a different mechanism operating. In addition, the phase composition of the gas nitrided layer was identified, based on X-ray diffraction (XRD) analyses, as AlN, Fe_4N, Fe_2N_{1-x} and α-Fe with no FeAl phase. However, it should be indicated that this conflicts with the findings of Pedraza et al. [22] that FeAl was still the matrix of the nitrogen implanted layer. Indeed, it is difficult, if not impossible, to distinguish between ordered B2 FeAl and α-Fe using XRD analyses alone because both the phases have similar lattice parameters.

Therefore, it is a timely task from both a scientific and technological point of view to systematically plasma-nitride the B2 FeAl alloy and fully characterize the microstructure of the nitride surfaces in order to investigate the response of B2 FeAl alloy to plasma-nitriding and to advance the scientific understanding of the mechanism involved. In this study, a FeAl40 aluminide was plasma-nitrided at temperatures ranging from 450 to 700 °C for 1–20 h in three different gas mixtures. The surface morphologies and roughness were observed; the depth distribution of chemical composition and microhardness across the nitride cases were measured and the kinetics of the formation of the nitride cases was studied. Systematically microstructural characterization was conducted using scanning electron microscopy (SEM), energy-dispersive X-ray spectroscopy (EDX), XRD and transmission electron microscopy (TEM). Based on the results, some interesting findings are discussed and the plasma-nitriding mechanism of FeAl40 aluminide is proposed.

2. Experimental

2.1. Material and plasma-nitriding

An iron-based Grade 3 FeAl40 (Fe–40 at.% Al) intermetallic alloy, provided by Centre de Recherche en Materiaux (CEREM), Centre d'Etudes Atomiques (CEA), Grenoble, France was used as the substrate material for the study. It has a density of 5.9 g cm^{-3} and the following chemical compositions (in wt.%): 24Al, 0.11Zr, 0.0025B, 1.00Y_2O_3 and balance Fe. Coupons of 28 × 15 × 10 mm were wet-ground with SiC paper down to 1200 grit, followed by polishing with 3 μm diamond paste and finished by fine polishing with a 0.25 μm colloidal silica.

Plasma-nitriding was carried out in a 60 kW Klöchner DC plasma furnace at a pressure of 5 mbar. A DC voltage from 300 to 1000 V was applied between the sample (cathode) and the wall of the furnace (anode) during the process. The treatment temperature was measured with a thermocouple. A wide range of treatment conditions (see Table 1) was designed to investigate the effect of temperature, time and gas composition. As listed in Table 1, six batches of samples were plasma-nitrided at temperatures ranging from 450 to 700 °C for 10 h with a gas mixture of 25% N_2 and 75% H_2 to study the temperature effect; three batches of samples were treated at 550 °C for 5, 10 and 15 h in a gas mixture of 25% N_2 and 75% H_2 in order to study the time effect; and the effect of gas composition was investigated using two different mixtures of gas compositions, 25% N_2 + 75% H_2 and 25% N_2 + 75% Ar. One additional batch of samples was treated at 550 °C for 10 h with 75% N_2 + 25% Ar gas mixture. Detailed treatment conditions and the sample code are listed in Table 1.

2.2. Surface layer characterization

The phase constitution of the plasma-nitrided layers was identified by XRD (Philips X'pert X-ray diffractometer) using a Cu-K_α radiation ($\lambda = 0.154$ nm). The chemical compositions of the layers were analysed using glow dis-

Table 1. Sample code and process parameters of plasma-nitriding treatments.

Sample code*	Temperature (°C)	Time (h)	Gas mixture		
			N_2 (%)	H_2 (%)	Ar (%)
T700t10	700	10	25	75	–
T600t10	600				
T550t10	550				
T500t10	500				
T470t10	470				
T450t10	450				
T550t5	550	5			
T550t10		10			
T550t15		15			
T550t1Ar	550	1	25	–	75
T550t5Ar		5			
T550t10Ar		10			
T550t20Ar		20			
T550t10N75Ar		10	75	–	25
I0	Untreated				

* Denotation in the sample code: T, temperature; t, time; N, nitrogen; Ar, argon.

charge spectroscopy (GDS; LECO GDS-750 QDP), which allowed for continuous depth-profiling for Fe, Al and N. The surface morphologies of the plasma-nitrided specimens were observed under SEM (Philips XL30). Metallographically prepared cross-section samples without etching were used for microhardness profiling using a Vickers microhardness tester (Mitutoyo MVK-H1) under a load of 25 g. Specimens were etched in Kellers solution (2 ml hydrofluoric acid, 5 ml nitric acid, 3 ml hydrochloric acid and 100 ml water) for layer structure observation by SEM. An EDX facility adapted to the SEM was used for the localized composition analysis during the observation.

2.3. TEM studies

Plan-view TEM specimens were prepared for as-received material and plasma-nitrided T700t10 samples to study the microstructure change during plasma-nitriding. The samples were cut and mechanically thinned from the substrate side to ≈50 μm in thickness, and then a 3 mm diameter disc was punched off. The discs were further reduced to ≈20 μm by a Gaton grinder, and they were then cut into two halves through the disc's diameter. Final thinning was carried out in a dual-beam FIB/SEM (Quanta 3D field emission gun focused ion beam miller). Prior to milling, a tungsten coating was deposited along the surface of the region where the sample was to be thinned. Milling was performed at 30 kV with currents from 15 nA to 5 nA, followed by final thinning at 30 kV with currents from 1 nA to 0.1 nA and finished with a final polish milling at 5 kV with 48 pA.

3. Results

3.1. Surface roughness and morphology

After plasma-nitriding treatments under different processing conditions, the original shining greyish colour of the specimens was changed to varying bands of dark brownish. Generally, the higher the treatment temperature and the longer the time, the rougher the specimen surfaces were. Fig. 1 shows the surface roughness (R_a) of the samples plasma-nitrided at 550 °C in a gas mixture of 25% N_2 + 75% Ar as a function of the treatment time. As seen in Fig. 1, R_a increased linearly with the treatment time up to 10 h, and then the increase in R_a slowed down when further increasing the treatment time to 20 h. Comparing the samples treated at the same temperature of 500 °C and for the same time of 5 h but with different gas mixtures of N_2 and Ar (T550t10Ar v. T550t10N75Ar), it was revealed that the R_a value was reduced from 0.30 for the sample treated in 25% N_2 + 75% Ar (T550t10Ar) to 0.13 when treated in 75% N_2 + 25% Ar (T550t10N75Ar), as shown in Fig. 1.

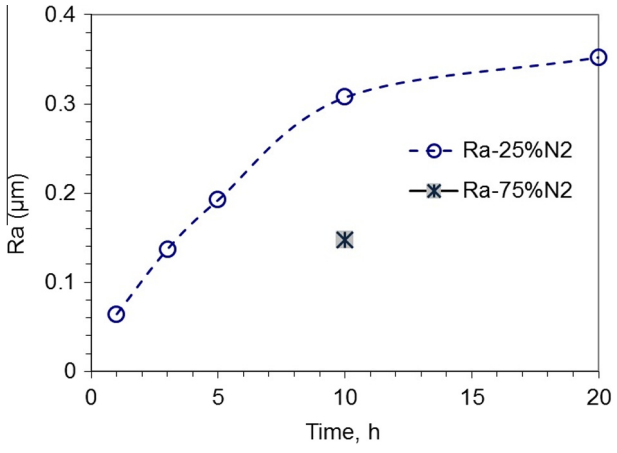

Fig. 1. Surface roughness of specimens treated at 550 °C in a gas mixture of N_2 + Ar as a function of treatment time.

SEM observations on the surface morphology of treated samples showed three types of surface features. The first group of samples revealed fine small particles in the size of 0.2–0.5 μm, as shown in Fig. 2a, which represents the samples treated below 500 °C or at 550 °C for less than 10 h. The second type of surface morphology observed on the samples treated for 10 h and more at 550 °C and 600 °C was composed of breadcrumb-like particles of size 0.5–3 μm (Fig. 2b), which resulted in a high R_a value of 0.3 μm. The third type of surface morphology was found for the 700 °C treated samples. As can be seen in Fig. 2c, the surface formed a dense layer, embedded with fine spherical particles and bubble-like large particles.

3.2. Surface layer structure

SEM observations on all cross-sectionally prepared nitride samples revealed that a surface layer was formed during plasma-nitriding. As can be seen in Fig. 3a and b, the surface layer features a dark contrasted matrix embedded with light contrasted wave shape lines. However, different interface features were observed: a straight, parallel to the surface interface was found for all low-temperature (⩽500 °C) treated samples (Fig. 3a) whilst a zigzagged interface was found for 600 °C and 700 °C treated samples (Fig. 3b). Fig. 3c shows an SEM image of a fractured sample. It can be seen from Fig. 3c that the fracture surface of the nitrided layer is much smoother and denser than the substrate, in contrast to the plastically fractured substrate material. Those white wave-lines observed in Fig. 3a and b can still be seen on the fracture surface, indicating the difference in hardness and hence deformation behaviour between these lines and the adjacent nitride layer matrix.

3.3. Thickness and microhardness of the nitrided layer

The thickness of the nitride layer was measured from the cross-sections using SEM, which was supported by the results obtained by GDS depth profiling. The growth of the nitrided layer was significantly influenced by the processing parameters.

For a fixed treatment time (i.e. 10 h in 25% N_2 + 75% H_2), the thickness of the nitrided layer increased steadily with temperature and peaked at ~75 μm when treated at 600 °C (Fig. 4a). However, the case thickness dropped sharply to 30–35 m at the temperature of 700 °C from more than 70 μm at 600 °C, which will be discussed in Section 4.

For a fixed treatment temperature of 550 °C, the thickness of the nitrided layer increased nearly linearly against the square root of time ($min^{1/2}$) regardless of the atmosphere used (Fig. 4b). It can also be found that the thickness of the nitride layer for those samples treated in a gas mixture of 25% N_2 + 75% H_2 was generally thicker than those nitrided in a gas mixture of 25% N_2 + 75% Ar.

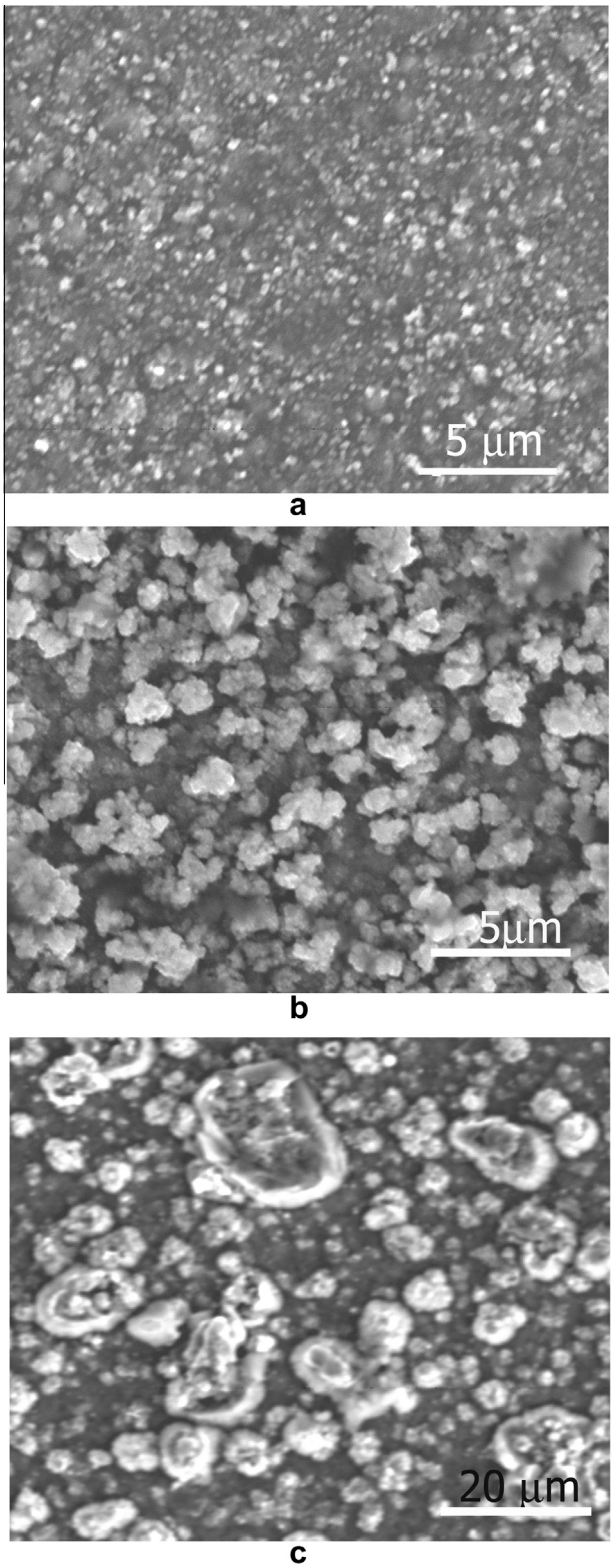

Fig. 2. Surface morphologies of specimens nitrided under different conditions: (a) T550t5Ar, 550 °C with 25% N_2 + 75% Ar for 1 h, (b) T550t10, 550 °C with 25% N_2 + 75% H_2 for 10 h and (c) T700t10, 700 °C with 25% N_2 + 75% H_2 for 10 h.

As illustrated in Fig. 4c, the surface hardness of all FeAl40 samples was increased significantly after plasma-nitriding in comparison with that of the untreated material. The microhardness plotted against the depth of the nitrided layer is shown in Fig. 4c and it can be seen that the microhardness is almost constant across the nitrided case; but it is noticeable that the microhardness of the 700 °C nitrided case is relatively lower than that of the other nitride samples. It is also found from Fig. 4c that in general the thickness of the nitride case increases with the treatment temperature but the nitride case formed on the 700 °C treated sample is much thinner than that of any other treated samples.

3.4. Composition depth distribution

A typical elemental distribution of nitrogen, iron and aluminium with depth is displayed in Fig. 5. Nitrogen peaks at the surface and decreases gradually in the near surface region before it levels off until the interface. After crossing the interface, the concentration of nitrogen drops sharply from the nitrided layer to the substrate and there is a narrow diffusion zone under the interface. In contrast, iron and aluminium contents start low and then level off in the nitride layer before climbing up across the interface to the matrix. The ratios of N/Al and N/Fe are ~1.15 and 0.70, respectively, in the nitride layer. The elemental distributions of the samples treated under other conditions show a similar trend to that shown in Fig. 5. An EDX line scan was used to study the elemental information across the white-contrasted wave-lines in the nitride layer, as indicated in Fig. 6a. It can be seen from Fig. 6b that the wave-line regions are rich in iron and lean in aluminium and nitrogen.

3.5. Phase constitution of the nitrided layers

3.5.1. XRD analysis

The XRD patterns of the samples plasma-nitrided at 500, 600 and 700 °C for 10 h in a gas mixture of 25% N_2 + 75% H_2 and the as-received FeAl40 sample are shown in Fig. 7a for comparison. The typical B2 (ordered body-centred cubic (bcc) structure) phase of FeAl alloy was identified as denoted by the dashed lines in the XRD patterns. Compared with the untreated sample, the plasma-nitrided samples contained a similar bcc phase but the peaks were shifted to the right of the B2 main bcc peaks of the untreated material. In addition, a nitride phase of AlN (ASTM03-065-0832) was detected for all the nitrided samples. This implies that a certain amount of Al may have been rejected from the B2 structure to combine with nitrogen to form AlN during the plasma treatments and the remaining iron atoms would form bcc ferrite with a smaller crystal constant than B2 as Al possesses a larger atom size (0.143 nm) than Fe atom (0.128 nm).

XRD patterns of three samples plasma-nitrided at 550 °C for 10 h with different gas compositions, i.e. 25% N_2 + 75% H_2 for T550t10, 25% N_2 + 75% Ar for T550t10Ar and 75% N_2 + 25% Ar for T550t10N75Ar, are shown in Fig. 7b, with the untreated sample as a reference. It can be seen that when treated using 25% N_2 + 75% H_2, only AlN was identified in the plasma-nitrided T550t10 sample. When the hydrogen was replaced by argon, i.e. using 25% N_2 + 75% Ar, not only AlN but also Fe_4N was formed (denoted by the dash-dot lines in Fig. 7b) in the plasma-nitrided T550t10Ar sample. A similar XRD pattern, or phase constitution, was observed for the T550t10N75Ar sample treated with 75% N_2 + 25% A These observations indicate that the replacement of hydro-

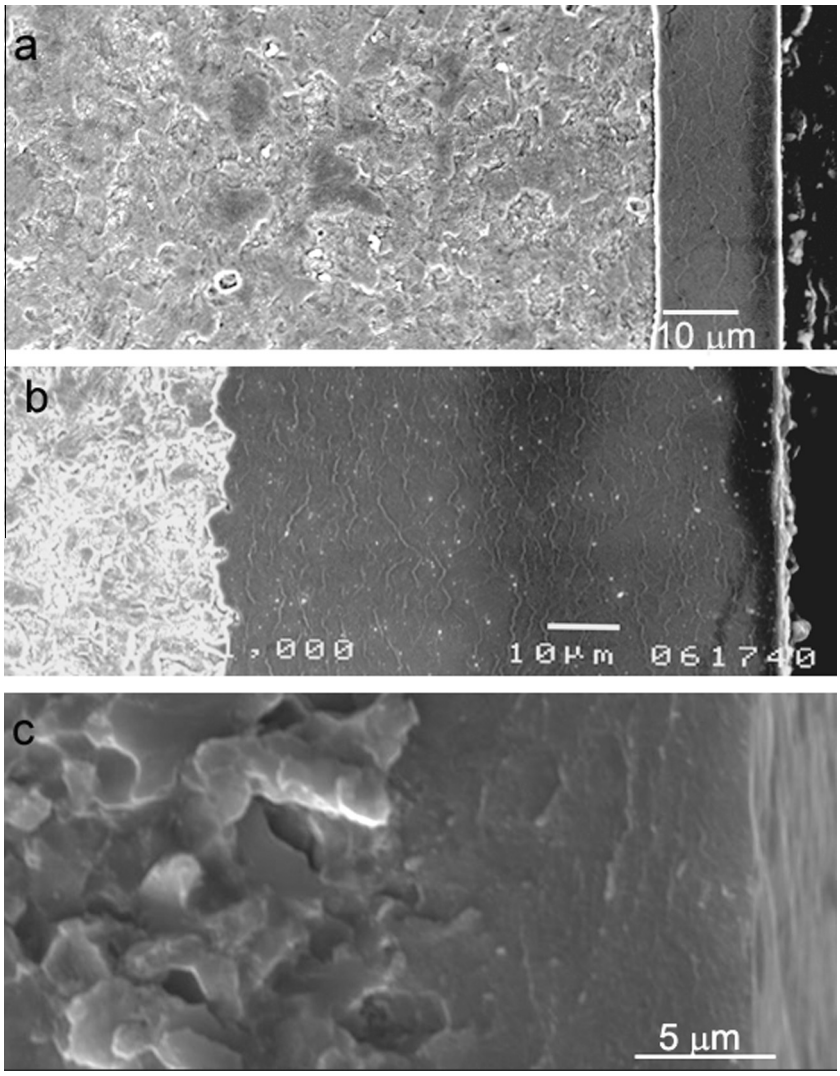

Fig. 3. SEM cross-section images of nitrided specimens: (a) T550t1Ar, nitrided at 550 °C in 25% N_2 + 75% Ar for 5 h, (b) T600t10, nitrided at 600 °C in 25% N_2 + 75% H_2 for 10 h and (c) fractured surface of T700t10, nitrided at 700 °C in 25% N_2 + 75% H_2 for 10 h.

gen by argon in the gas mixture promoted the formation of Fe_4N iron nitride. This might be due to the fact that the lighter hydrogen ions are easier to be absorbed in the surface in comparison to the heavy argon ions, which discounts the relative amount of nitrogen ions absorbed in the surface, reducing the reacting opportunities of iron with nitrogen [24].

3.5.2. TEM characterization

Fig. 8 shows a TEM microstructure and a corresponding selected area diffraction (SAD) pattern for as-received material. It can be seen that the microstructure of the as-received material consisted of equiaxed grains of size 1–5 μm (Fig. 8a) with an ordered B2 structure, as evidenced in Fig. 8b by the [100] zone SAD pattern.

A TEM study of a plasma-nitrided T700t10 sample was carried out within the plasma-nitrided case. TEM observations revealed that in the nitride layer, the majority of the original B2 phase grains was decomposed into a mixed microstructure with fine needles embedded in the matrix, as shown in Fig. 9a. Analysing the SAD patterns taken from the nitride layer revealed AlN (ASTM03-065-0832, $a = 0.311$ nm, $c = 0.498$ nm) and α-Fe (bcc, $a = 0.308$ nm), which is consistent with the d-spacing from the XRD pattern of this sample. It follows that when nitrogen diffused into FeAl during the plasma-nitriding, AlN was precipitated from the original ordered B2 grains, which resulted in the decomposition of ordered B2 into bcc α-Fe. Accordingly, a fine lamellar structure consisting of AlN and α-Fe was formed in the plasma-nitride layer. As shown in Fig. 9a, the original B2 grain boundaries are very sharp without visible inter-granular zones, as denoted by dotted lines in Fig. 9a. This indicated that the wave-lines observed in the nitride layer under SEM are not connected to the original B2 grain boundaries. Instead, detailed TEM observation revealed that wave-lines were formed within the original B2 grains. Fig. 10a shows a cross-sectional view of the wave-line (denoted by an arrow and dotted lines) and the plan view of the wave-line showed a few grains of α-Fe (Fig. 10b, denoted by a white loop), as evidenced by the SAD pattern (Fig. 10c) taken from one of the grains in the enclosed area shown in Fig. 10b.

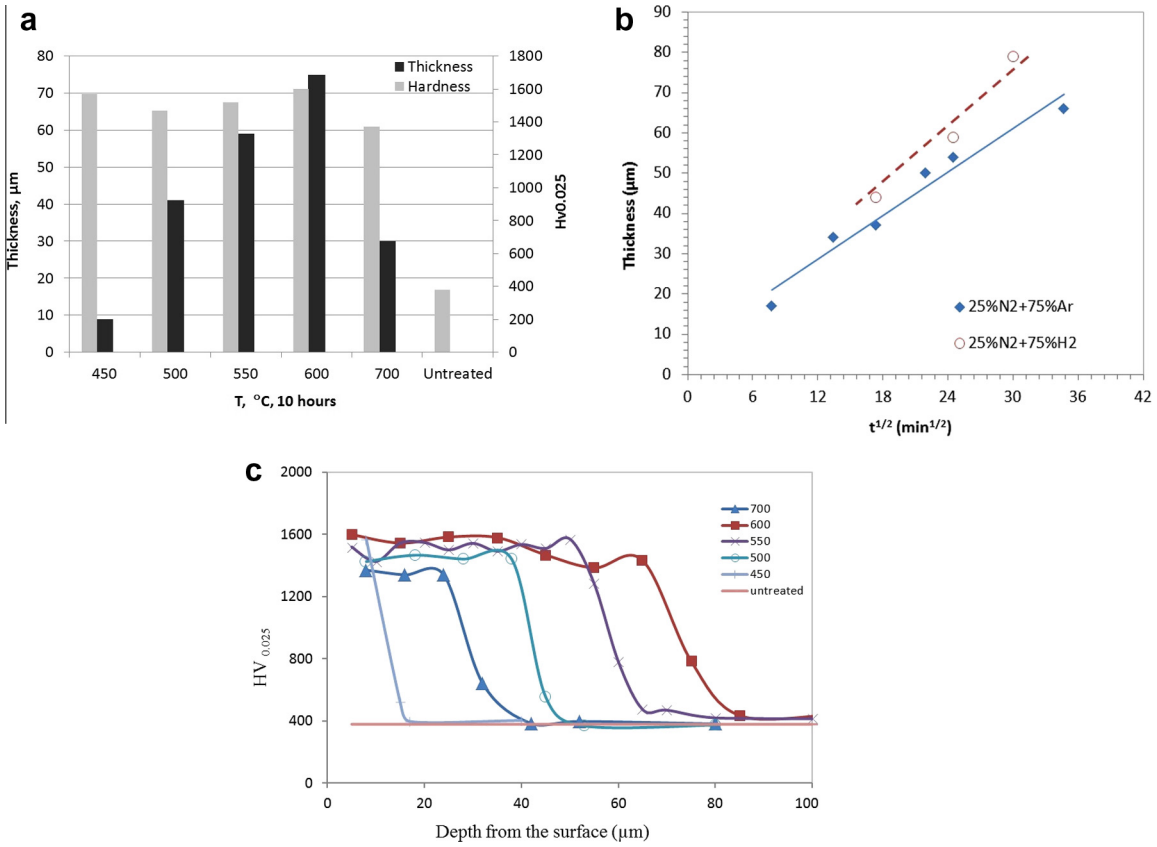

Fig. 4. (a) The effect of process temperatures on the thickness and surface microhardness of nitrided layers; (b) the relationship between the thickness of the nitride layer and the square root of time in two different atmospheres and (c) the hardness depth profiles of the samples treated at different temperatures in comparison with the untreated sample.

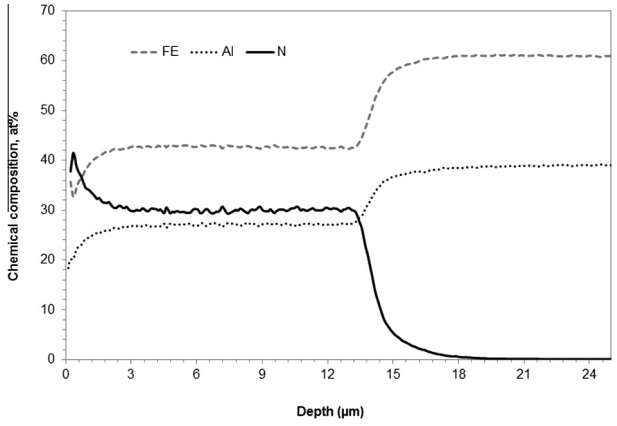

Fig. 5. Typical glow discharge optical emission spectroscopy depth profiles of chemical composition of a surface-nitrided T550t1Ar sample.

4. Discussion

Two scientifically interesting findings, i.e. (i) the formation of wave-like lines in the nitride case and (ii) the case thickness of 700 °C treated T700t10 is much thinner than that of 600 °C treated T600t10 sample, have been reported above, which are worth further study to advance scientific understanding.

4.1. Formation of wave-like lines in the nitride cases

The wave-like lines observed in the plasma-nitrided case as shown in Fig. 3 were also reported by Spies et al. [23] in the gas-nitrided case of FeAl. They believed that the wave-like lines might be related to the formation of nitrides along the original grain boundaries of FeAl during nitriding. However, the EDX line scanning carried out in this study has clearly indicated that these wave-like line features are indeed lean in N and rich in Fe (Fig. 6). Therefore, the formation mechanism of these wave-like line features needs to be investigated further.

During plasma-nitriding, a high voltage electrical energy is used to form a plasma in a vacuum, through which nitrogen ions are accelerated to impinge on the sample, clean the surface and provide active nitrogen species [25]. It is well known that diffusion of nitrogen is much faster along grain boundaries than through the bulk grains, i.e. short-circuit diffusion. Hence, nitrogen would preferentially diffuse along grain boundaries (Fig. 11a).

Among all the alloying elements in FeAl40 alloy, aluminium has the highest chemical activity. This is partially because, although Zr and B have a much stronger chemical affinity to N when compared with Al, the concentration of Al (24 wt.%) is much higher than that of Zr (0.11 wt.%) and B (0.0025 wt.%) and partially because the chemical affinity of N to Al is much stronger than to Fe even if the material contains more Fe (~75 wt.%) than Al (24 wt.%). Hence, when nitrogen further diffuses from the grain boundaries

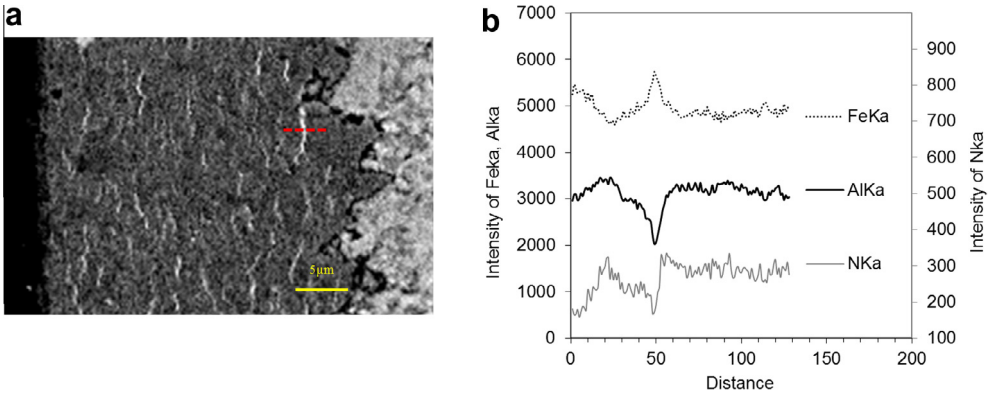

Fig. 6. An EDX line scan across the wave-line in the nitride layer (T700t10): (a) SEM image showing the location of the line, (b) the distribution of Fe, Al and N.

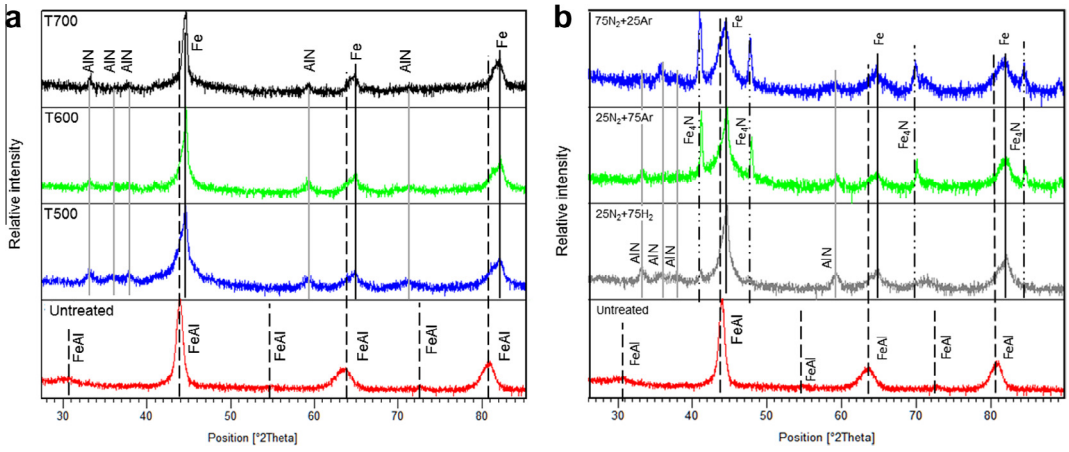

Fig. 7. XRD patterns of untreated and plasma-nitrided samples: (a) treated at different temperatures with 25% N_2 + 75% H_2 for 10 h and (b) treated at 550 °C for 10 h in different gas mixtures.

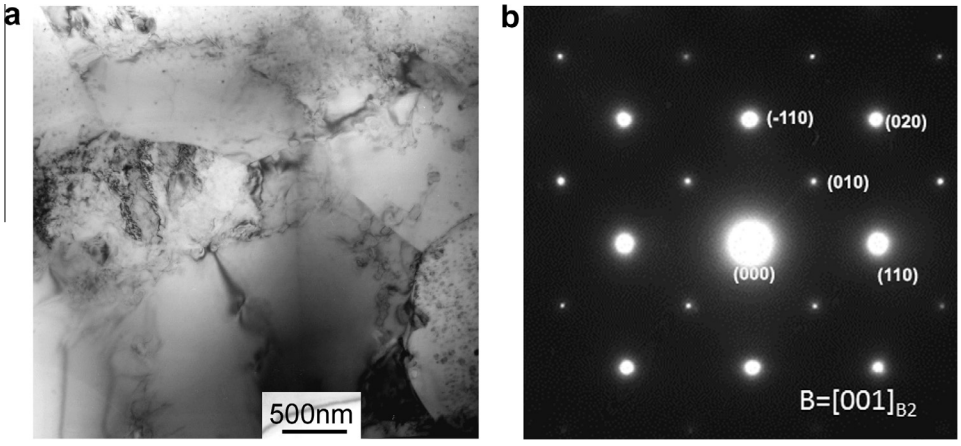

Fig. 8. TEM microstructure of (a) as-received FeAl40 and (b) a corresponding SAD pattern.

towards the centre of grains, Al would diffuse towards the grain boundaries and react with the activated nitrogen ions to form hexagonal wurtzite crystal structure type AlN needles at the early stage of nitriding (Fig. 11b). The formation of AlN needles consumes aluminium in the FeAl matrix and thus the areas adjacent to the AlN needles are lean in Al and rich in Fe. This leads to the decomposition of the ordered B2 FeAl and the generation of α-Fe between the AlN needles, hence the formation of a lamellar microstructure of AlN/α-Fe (Fig. 11c). When nitrogen diffuses further towards the core of original FeAl grains where there is plenty of aluminium for the growth of AlN needles, bundles of AlN needles and hence the lamellar structure of AlN/α-Fe are progressively taking shape as schematically

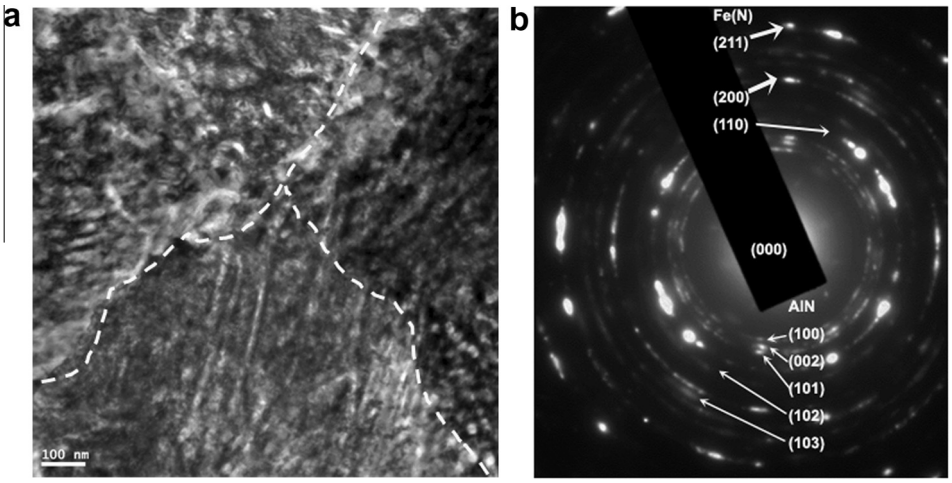

Fig. 9. TEM microstructure of (a) plasma-nitrided layer for sample (T700t10) and (b) a corresponding SAD pattern.

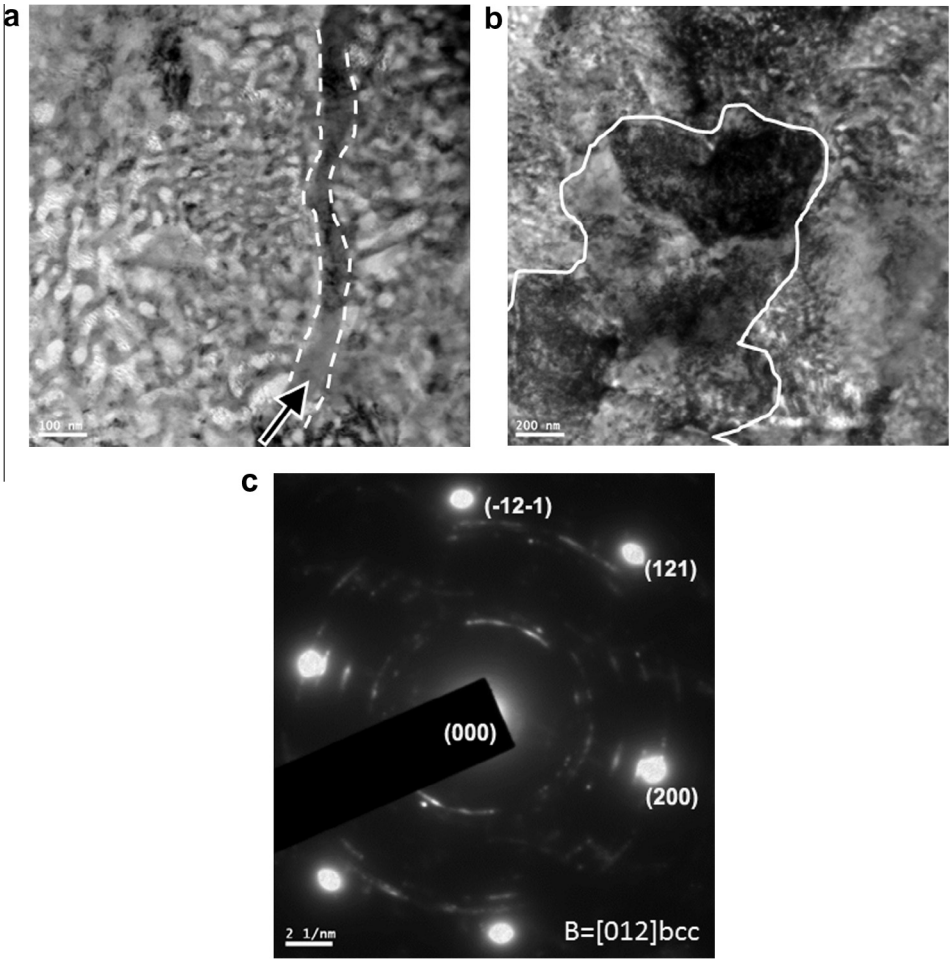

Fig. 10. TEM microstructure of (a) cross-sectional view of the wave-line; (b) the plan view of the wave-line and (c) the corresponding SAD pattern from plasma-nitrided sample T700t10.

shown in Fig. 11d. In the meantime, the strong chemical affinity between nitrogen and aluminium also attracts aluminium in the central region of grains to diffuse outward to react with nitrogen. This leaves behind an Al-depleted and Fe-enriched region within the centre of theses grains. Because the grains are in equiaxial shape with wave-like grain boundaries and the perpendicular diffusion direction of nitrogen from grain boundaries, the final Fe-enriched and Al-depleted regions in the centre of these grains would take the form of wave-like lines (Fig. 11d). Hence, the proposed formation mechanism can be summarized in Fig. 11. This has been confirmed by an EDX line scan across the

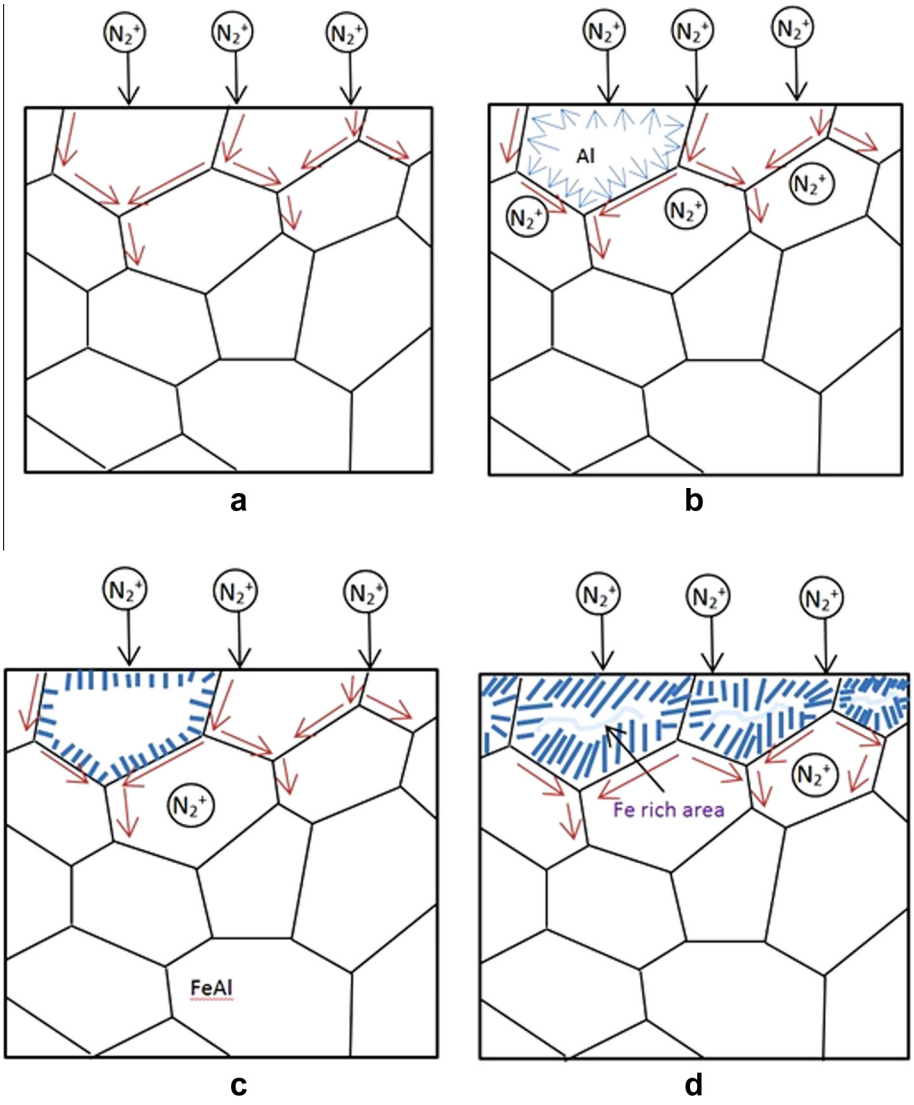

Fig. 11. Schematic illustrations of wave-line forming mechanism for plasma-nitriding iron aluminude.

white line of the nitride layer (Fig. 6b) and further proved by the TEM images as displayed in Fig. 10a and c.

With the progress of nitriding, nitrogen diffuses further down the surface, and a continuous nitride layer with wave-like white lines is formed, as demonstrated in Fig. 3a and b. The continuous supply of nitrogen from the plasma is responsible for the nitrogen peak at the surface (as seen in Fig. 5), which is the initial driving force for nitrogen diffusion inward in the nitride case. As is shown in Fig. 5, the nitrogen content within the nitride layer exceeds the amount which is required for the formation of AlN (>1), and the excess nitrogen is trapped at dislocations, absorbed at precipitate–matrix interfaces and dissolved in the α-Fe. Nitrogen content levels off in the nitride layer (Fig. 5), mainly due to the reaction–diffusion nature (Fig. 5b). A sharp drop of nitrogen content at the interface of the nitride layer and matrix indicates the formation of a shallow diffusion zone.

4.2. Abnormal growth kinetics of the 700 °C nitride case

As has been shown in Fig. 4c, the thickness of the nitride layer of the 700 °C treated T700t10 sample is less than half the thickness of the 600 °C treated T600t10 sample. The anomaly of temperature effect on the growth of the nitrided case was also reported by Spies et al. during gas nitriding [23]. They attributed this abnormal growth kinetics to the decreased nitrogen potential ($K_N = (P_{(NH_3)}/P_{H_2})^{3/2}$) at elevated temperature due to the temperature-dependent decomposition of NH_3. However, this assumption could not be used to explain the anomaly observed in plasma-nitriding because N_2 rather than NH_3 (hence no NH_3 decomposition) is used in the plasma-nitriding process.

In order to find the mechanism involved in the observed abnormal growth kinetics of the 700 °C nitride case, further elemental analysis by EDX of T700t10 had been conducted and a higher level of oxygen and aluminium was detected at the surface in comparison with other samples, as shown in Fig. 12a. No separate oxygen peak can be identified at the surface and the aluminium peak is overshadowed by an iron peak for the sample treated at 550 °C (T550t10, Fig. 12b); however, the oxygen peak is pronounced and the intensity of Al is even higher than that of Fe for those samples treated at 700 °C. It is reasonably speculated that a continuous alumina layer was formed at 700 °C on the very surface region although it cannot be clearly identified from

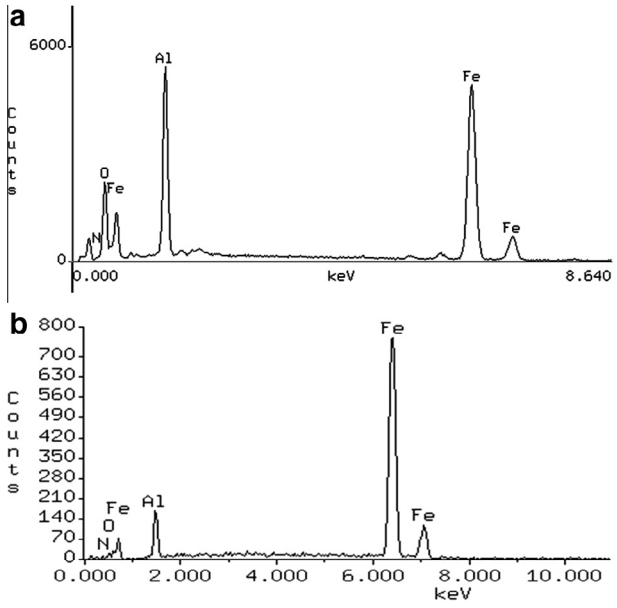

Fig. 12. EDX analysis of surface composition for plasma-nitrided under (a) 700 °C/10 h (T700t10) and (b) 550 °C/10 h (T550t10) specimens in a gas mixture of 25% N_2 + 75% H_2.

the XRD pattern. This is presumably partially because the alumina oxide film is too thin to be detected by XRD and partially because the structure of alumina is the same as the bulk nitride layer and thus the overlapping of some peaks of Al_2O_3 with those of AlN. It is known that a surface oxide layer can act as a barrier layer to inhibit further intake of nitrogen and thus greatly reduce the growth of nitride case (Fig. 4a and c) and the amount of nitrogen in the nitride layer and hence the hardness value (Fig. 4c).

The onset of oxidation of AlN normally lies between 700 and 800 °C but under certain conditions, a stable α-Al_2O_3 can be formed below 700 °C [26,27]. The oxidation of AlN can be written as follows:

$$4AlN + 3O_2(g) \rightarrow 2Al_2O_3 + 2N_2(g)$$

The Gibbs free energy change of the oxidation ΔG and the standard Gibbs free energy change ΔG° between 327 and 1327 °C are given by Lin and Lu [27]:

$$\Delta G = \Delta G^{\circ} + RT\ln\left(\frac{P_{N_2}^{2/3}}{P_{O_2}}\right)$$

$$= -RT\ln\left(\frac{P_{N_2}^{2/3}}{P_{O_2}}\right)_{equil.} + RT\ln\left(\frac{P_{N_2}^{2/3}}{P_{O_2}}\right)$$

$$= [-690 + 0.064 \times T] + \frac{RT}{1000}\ln\left(\frac{P_{N_2}^{2/3}}{P_{O_2}}\right) \text{ (kJ/mol)}$$

where R is the gas constant (8.31 J mol^{-1} K^{-1}), T is the annealing temperature (K), P_{N_2} and P_{O_2} are the specific nitrogen and oxygen partial pressures, respectively, in the gas mixture and $((P_{N2}^{2/3})P_{O_2}\cdot)$equil. is the specific nitrogen and oxygen partial pressure ratio at which AlN is in thermodynamic equilibrium with Al_2O_3. From the calculations, $\Delta G \ll 0$ if the gas mixture contains a minute amount of oxygen, and this is also depends on the temperature.

Indeed, some difficult-to-nitride materials such as titanium and aluminium alloys have put their blame on the formation of a protective surficial oxide layer. Sun [28] attributed the anomaly kinetics of nitriding of Inconel 600 (nitriding layer became thinner when treated at a higher temperature) to the impeding effect of the superficial chromium/iron oxynitride on nitrogen mass transfer. Similarly, Dang et al. found that α-Al_2O_3 was responsible for the decrease in the mass gain of an ion-nitriding-treated B2 iron aluminide at high temperature [29]. It thus follows that there would be a critical temperature between 650 and 700 °C, where nitride, especially AlN, is oxidized due to the small amount of impurity oxygen in the gas mixture or relatively low vacuum used as in this study. A continuous thin oxide layer is produced to act as a barrier for nitrogen mass transfer, hence changing the nitriding dynamics, which adversely affects the nitrogen intaking and nitride layer growth.

5. Summary and conclusions

FeAl40 has a good response (in terms of layer formation and hardening) to plasma-nitriding at temperatures between 450 and 600 °C. After plasma-nitriding, a thick nitride case plus a shallow diffusion zone was formed.

The thickness of plasma-nitride layer increased with treatment temperature and time when treated at 600 °C or below and the surface hardness of FeAl40 was significantly increased to 1400–1500 $HV_{0.025}$. Further increasing the treatment temperature to 700 °C reduced both the hardness and thickness of the nitride case, presumably due to the formation of surface aluminium oxide.

Detailed studies using SEM/EDX, XRD and TEM revealed that AlN was preferably formed during plasma-nitriding of FeAl40; meanwhile the original B2 phase grains were decomposed into a lamellar structure, consisting of fine AlN needles embedded in the α-Fe matrix, and wave-like featured α-Fe grains were found in the centre of original B2 grains. Based on the experimental results, a model for the formation of the wave-like line features within the plasma-nitride layers has been proposed.

The composition of the gas mixture affected the composition and thickness of the nitride cases. When a gas mixture of nitrogen and hydrogen was used, only AlN was formed in the nitride layer; however, the use of a gas mixture of nitrogen and argon led to the formation of both AlN and Fe_4N in a relatively thin nitride layer.

Acknowledgement

This project was sponsored by the EPSRC UK (GR/N13807/01).

References

[1] C.T. Liu, E.P. George, P.J. Maziasz, J.H. Schneibel, Mater. Sci. Eng., A 258 (1998) 84–98.
[2] N.S. Stoloff, V.K. Sikka, Physical Metallurgy and Processing of Intermetallic Compounds, Chapman & Hall, London, 1996.
[3] B. Xu, Z. Zhu, S. Ma, W. Zhang, W. Liu, Wear 257 (2004) 1089–1095.
[4] B. Benjamin, S. Michael, P. Christoph, M. Frank, Surf. Coat. Technol. 235 (2013) 773–777.
[5] L. Sánchez, F.J. Bolívar, M.P. Hierro, F.J. Pérez, Intermetallics 16 (2008) 1161–1166.

[6] R. Łyszkowski, J. Bystrzycki, T. Płociński, Intermetallics 18 (2010) 1344–1347.
[7] P.Z. Shen, Y.H. He, H.Y. Gao, J. Zou, N.P. Xu, Y. Jiang, B.Y. Huang, C.T. Liu, Desalination 249 (2009) 29–33.
[8] H. Song, Y. Wu, C. Tang, S. Yuan, Q. Gong, J. Liang, Tsinghua Sci. Technol. 14 (2009) 300–306.
[9] S. Azem, M. Nechiche, K. Taibi, Powder Technol. 208 (2011) 515–520.
[10] D.G. Morris, M.A. Muñoz-Morris, J. Alloys Compd. 536 (Supplement 1) (2012) S180–S185.
[11] M.A. Montealegre, J.L. González-Carrasco, M.A. Morris-Muñoz, J. Chao, D.G. Morris, Intermetallics 8 (2000) 439–446.
[12] N.S. Stoloff, C.T. Liu, S.C. Deevi, Intermetallics 8 (2000) 1313–1320.
[13] J. Qiu, I. Baker, F.E. Kennedy, Y. Liu, P.R. Munroe, Intermetallics 40 (2013) 19–27.
[14] H.E. Maupin, R.D. Wilson, J.A. Hawl, Wear 162–164 (1993) 432–440.
[15] K. Yong-Suk, K. Yong-Hwan, Mater. Sci. Eng., A 258 (1998) 319–324.
[16] P. Haušild, J. Siegl, P. Málek, V. Šíma, Intermetallics 17 (2009) 680–687.
[17] D.E. Alman, J.A. Hawk, J.H. Tylczak, C.P. Doğan, R.D. Wilson, Wear 251 (2001) 875–884.
[18] X. Li, H. Dong, 14 – Ceramic conversion treatment of titanium-based materials, in: H. Dong (Ed.), Surface Engineering of Light Alloys, Woodhead Publishing, 2010, pp. 475–500.
[19] J. Xia, C.X. Li, H. Dong, Wear 258 (2005) 1804–1812.
[20] E. Ekmekçiler, A. Polat, M. Usta, Surf. Coat. Technol. 202 (2008) 6011–6015.
[21] J.L.G.-P.F. Pedraza, J.F. Dinhut, Mater. High Temp. 22 (2005) 283–286.
[22] F. Pedraza, J.L. Grosseau-Poussard, J.F. Dinhut, Thin Solid Films 467 (2004) 140–145.
[23] H.J. Spies, H.H. Biermann, A. Fischer, Z. Metallkd. 96 (2005) 781–786.
[24] K.S. Jung, R.E. Schacherl, E. Bischoff, E.J. Mittemeijer, Philos. Mag. 91 (2011) 2382–2403.
[25] H.E. Maupin, R.D. Wilson, J.A. Hawk, Wear 162–164 (1993) 432–440, Part A.
[26] H. Zhou, L. Qiao, R. Fu, Mater. Res. Bull. 37 (2002) 2427–2435.
[27] C. Lin, F. Lu, J. Eur. Ceram. Soc. 28 (2008) 691–698.
[28] Y. Sun, J. Alloys Compd. 351 (2003) 241–247.
[29] C. Dang Ngoc Chan, C. Huvier, J.F. Dinhut, Surf. Coat. Technol. 165 (2003) 119–125.